doi: 10.18323/2782-4039-2024-2-68-1

Influence of high-pressure torsion on the structure and mechanical properties of Zn–1%Fe–5%Mg zinc alloy

Elmira D. Abdrakhmanova[1], student
Elvira D. Khafizova*[2], PhD (Engineering),
assistant professor of Chair of Materials Science and Physics of Metals,
senior researcher of Scientific Research Laboratory "Metals and Alloys under Extreme Impacts"
Milena V. Polenok[3], student
Ruslan K. Nafikov[4], junior researcher of Scientific Research Laboratory "Metals and Alloys under Extreme Impacts"
Elena A. Korznikova[5], Doctor of Sciences (Physics and Mathematics), Professor,
professor of Chair of Materials Science and Physics of Metals,
Head of Scientific Research Laboratory "Metals and Alloys under Extreme Impacts"
Ufa University of Science and Technology, Ufa (Russia)

***E-mail:** KhafizovaED@uust.ru, ela.90@mail.ru

[1]ORCID: https://orcid.org/0009-0009-2775-7488
[2]ORCID: https://orcid.org/0000-0002-4618-412X
[3]ORCID: https://orcid.org/0000-0001-9774-1689
[4]ORCID: https://orcid.org/0000-0003-1280-6258
[5]ORCID: https://orcid.org/0000-0002-5975-4849

Received 27.06.2023 *Accepted 06.03.2024*

Abstract: Currently, scientists search for new materials for temporary implants that can dissolve in the body, which leads to the fact that there is no need for repeated surgery. In the last decade, scientific interest has focused on zinc-based materials because, unlike other metals, it has suitable corrosion rates and good biocompatibility. The paper describes an experiment for the study of the influence of deformation on the microstructure, strength and corrosion properties of an alloy of the Zn–Fe–Mg system. The authors carried out energy dispersive analysis and calculation of the volume fraction of the second phase of the Zn–Fe–Mg zinc alloy. The corrosion properties of the Zn–Fe–Mg zinc alloy with different microstructures (before and after high-pressure torsion) were studied using the gravimetric method under conditions simulating conditions inside a living organism (temperature, corrosive environment composition). During the tests, the corrosion mechanism was determined, its rate and mass loss of the samples were calculated. The relief of the corrosion surface was studied using scanning electron microscopy. It has been found that the destruction of the material in a corrosive environment occurs through a matrix containing the active Mg metal. The results of calculations of the corrosion rate for the original sample and samples subjected to high-pressure torsion differed due to a more even distribution of second phase particles during severe plastic deformation. In this work, by alloying zinc with iron and magnesium, as well as using high-pressure torsion, it was possible to increase the microhardness of the samples to 239.6±8 HV, which is a high indicator for zinc alloys.

Keywords: zinc alloys; Zn–Fe–Mg; biodegradable implants; high-pressure torsion; biocompatible materials.

Acknowledgments: The research was financially supported by a grant in the field of science from the budget of the Republic of Bashkortostan for state support of young scientists (Scientific and Educational Center – Grant for Young Scientists – 2022, Agreement No. 1 of 13.12.2022).

The work of Korznikova E.A., Nafikov R.K. was carried out under financial support of the Ministry of Science and Higher Education of the Russian Federation within the state assignment for public service delivery given to Ufa University of Science and Technology (Agreement No. 075-03-2024-123/1) "Youth Science and Research Laboratory of Scientific and Educational Center "Metals and Alloys under Extreme Impacts".

The research part of the work was carried out using the equipment of the Core Facility Centre "Nanotech" of Ufa University of Science and Technology.

The paper was written on the reports of the participants of the XI International School of Physical Materials Science (SPM-2023), Togliatti, September 11–15, 2023.

For citation: Abdrakhmanova E.D., Khafizova E.D., Polenok M.V., Nafikov R.K., Korznikova E.A. Influence of high-pressure torsion on the structure and mechanical properties of Zn–1%Fe–5%Mg zinc alloy. *Frontier Materials & Technologies*, 2024, no. 2, pp. 9–22. DOI: 10.18323/2782-4039-2024-2-68-1.

INTRODUCTION

Currently, biodegradable materials are considered as temporary implants for osteosynthesis and vascular stenting. Biodegradable materials have certain advantages over implant materials traditionally used in medicine due to theirability to dissolve in the body. During research, it has been found that zinc alloys have better mechanical and corrosion properties than previously studied magnesium- and iron-based materials.

Zinc is an essential ion in many cellular and biochemical processes, and promotes accelerated wound healing [1], thereby reducing the body recovery time in the post-surgery period. Pure zinc is a rather brittle material with low hardness (38.24±1.06 HV), and it is impossible to consider it in its pure form as a material for the production of implants. Alloying is one of the main effective methods for improving the complex properties of pure Zn. A mandatory requirement for alloying elements of a material for the production of medical implants is their non-toxicity. An interesting combination is the alloying with Fe and Mg, since they are biodegradable metals and at the same time strengthen the alloy [2]. In vitro studies of magnesium alloys showed that Mg corrosion products are not harmful to cells [2], and in Zn–Mg alloys [3], the survival rate of MC3T3-E1 mouse cells is higher, but Zn–Fe turned out to be cytotoxic, although human umbilical vein endothelial cells (HUVECs) turned out to be biocompatible with it [3].

Iron in the solid state has insignificant solubility in the Zn matrix, which leads to the formation of large particles of the second phase and has a strengthening effect on the alloy [4]. This is why in this work, Fe was chosen as one of the alloying metals. In the Zn–Fe state diagram, the equilibrium phase composition at room temperature consists of Zn and $FeZn_{13}$ due to the negligible solubility of Fe in Zn in the solid state [5]. The Zn–0.4Fe zinc alloy demonstrates good mechanical properties and biocompatibility, however, it is reported that when the iron content in the alloy increases to 2.5 %, the ductility values sharply decrease due to an increase in the volume fraction of the intermetallic phase [6]. The Zn–Mg–Fe zinc alloy showed good compatibility in in vivo studies on beagle dogs [7]. Osteosynthesis plates were placed in the frontal bone, mandible, and astragalus. The Zn–Mg–Fe alloy degraded uniformly, without significant differences in the rate of degradation of the frontal, mandibular, and astragalus implants. The corrosion rate reached approximately 0.183 mm/year in the first 3 months and then decreased to approximately 0.065 mm/year after 12 months [7].

Magnesium is also an important cation playing a crucial role in many physiological functions, so it was chosen as one of the alloying metals. Previously, an alloy with magnesium concentrations from 0.15 to 3.0 wt. % was developed [8]. Increasing the Mg content increased the microhardness values and tensile strength of Zn–Mg alloys, as the volume fraction of the solid intermetallic Mg_2Zn_{11} phase increased. Zn–Mg system alloys have a structure consisting of primary zinc and an interdendritic eutectic mixture. This structure provides mechanical strength comparable to that of a human bone [9]. In fine-grained alloys, a change in the corrosion mechanism from pitted to more uniform due to the second phase refinement was observed. With an increase in the Mg amount in the Zn–Mg alloy composition, its cytocompatibility increases and more uniform corrosion is observed, while localized corrosion was observed in the alloy with iron [3].

Through alloying and severe plastic deformation, it is possible to increase the strength properties of the alloy and regulate the corrosion rate by changing the structure parameters. Controlling the material destruction rate is one of the important tasks, since corrosion products should not exceed the maximum permissible concentration in the human body. The implant should not be destroyed until the bone tissue is completely restored, and the stent should not be destroyed until the vessel is restored. It is known that a fine-grained structure is formed in a metal after treatment by high-pressure torsion (HPT), and grain refinement leads to improved mechanical properties [10].

Currently, the alloy of the Zn–Fe–Mg system is understudied. This work studies the Zn–1%Fe–5%Mg alloy subjected to high-pressure torsion.

The purpose of the work is to study the influence of high-pressure torsion on the structure and mechanical properties of the Zn–1%Fe–5%Mg zinc alloy.

METHODS

The research material is the Zn–1%Fe–5%Mg alloy (Table 1). The chemical composition was determined on a Thermo Scientific ARL Optim'X X-ray fluorescence spectrometer. Melting was carried out in a chamber furnace in a graphite crucible with a diameter of 20 mm with a lid at a temperature of 580 °C. After that, the samples were subjected to homogenizing annealing at a temperature of 350 °C for 12 h.

Disks with a diameter of 20 mm and a thickness of 1.8 mm were cut on an ARTA 120 CNC electrical discharge machine. The disks were sanded using waterproof sanding paper of various grits. After that, the samples were subjected to high-pressure torsion in a SKRUDZH-200 machine at room temperature with an upper striker pressure of 6 GPa. The number of torsion revolutions is 0.5–10. When deformed by torsion, the original and resulting samples had the shape of disks. Samples were examined in the initial state and after deformation.

Table 1. *Chemical composition of the Zn–1%Fe–5%Mg alloy, wt. %*
Таблица 1. *Химический состав сплава Zn–1%Fe–5%Mg, вес. %*

Content of chemical elements, wt. %			
Zn	**Fe**	**Mg**	**The rest**
92.72±0.13	0.911±0.045	5.32±0.11	1.049±0.030

Static tensile tests were carried out on small samples (Fig. 1) on an Instron 5982 electromechanical measuring system at room temperature and a speed of 0.24 mm/min. The length of the test specimens was 10 mm, thickness – 0.8 mm, and neck thickness – 1 mm.

The microhardness of deformed samples was determined using an EMCO-Test DuraJet 10 hardness tester using the Vickers method (GOST 9450–76) under a load of 0.1 kg. The values were studied at 20 points with a step of 1 mm along the entire diameter of the sample.

Studies of the structure, the corrosion surface relief and analysis using energy dispersive X-ray spectroscopy (EDS) were carried out using a JEOL JSM-6490LV scanning electron microscope.

To study the structure, the samples were preliminarily etched in a 15 % sulfuric acid solution for 10 s. Calculations of the volume fraction of the second phase in zinc alloys were performed using the ImageJ program.

Corrosion tests were carried out for 60 days using the gravimetric method in accordance with the ASTM G1-03-E standard. Samples were studied in the initial state and after high-pressure torsion for 10 revolutions. At least 3 samples were taken for each state. The tests included exposing the samples to a corrosive environment – Ringer's solution (composition: 8.6 g/l of NaCl; 0.3 g/l of KCl; 0.25 g/l of $CaCl_2$, saline solution pH 7). The tests were carried out at a constant temperature of 38±1 °C.

The samples were weighed and photographed before and after cleaning from corrosion products every 2 days. Cleaning from corrosion products was carried out in a VI chromium oxide solution (200 g of reagent per 1000 ml of distilled water), then in distilled water using a KAISI-105 ultrasonic bath. After cleaning, the samples were dried and weighed on an EJ-123 electronic balance providing measurement accuracy of up to 0.01 mg. After cleaning from corrosion products and weighing, the samples were again kept in a corrosive environment. The surface of the samples was examined more closely by scanning electron microscopy every 14 days.

The corrosion rate *CR* mm/year was calculated according to the ASTM G3–63592 standard using the formula:

$$CR = \frac{87.6\,(M_0 - M_1)}{S\,t\,\rho},$$

where *CR* is the corrosion rate, mm/year;
S is the sample surface area, cm^2;
M_0 is the initial mass, mg;
M_1 is the mass after immersion, mg;
t is the holding time, h;
ρ is the metal density, g/cm^3.

Mass loss in % was calculated using the formula:

$$ML = \frac{(M_0 - M_1)}{M_0} \cdot 100\,\%,$$

where *ML* is the mass loss, %.

X-ray diffraction analysis (XRD) was carried out on a D2 Phaser desktop X-ray diffractometer with CuKα radiation at 30 kV and 10 mA with a shooting step of 0.02° and a scan rate of 1 °/min. X-ray phase analysis (XPA) of the obtained x-ray patterns was carried out in the Diffrac.Eva software package.

RESULTS

Structure and microhardness studies

The resulting alloy in the initial state had high microhardness values (210±4.6 HV). Samples after high-pressure torsion showed an uneven microhardness distribution over the entire diameter. The average microhardness values after high-pressure torsion are presented in Fig. 2, where after 2 torsion revolutions, a slight increase in microhardness to 239.6±8 HV is observed.

Studies of the structure have shown that in the initial state (Fig. 3 a) the alloy consists of a eutectic matrix with a fine-plate α-Zn and Mg_2Zn_{11} structure (Fig. 3 b), large

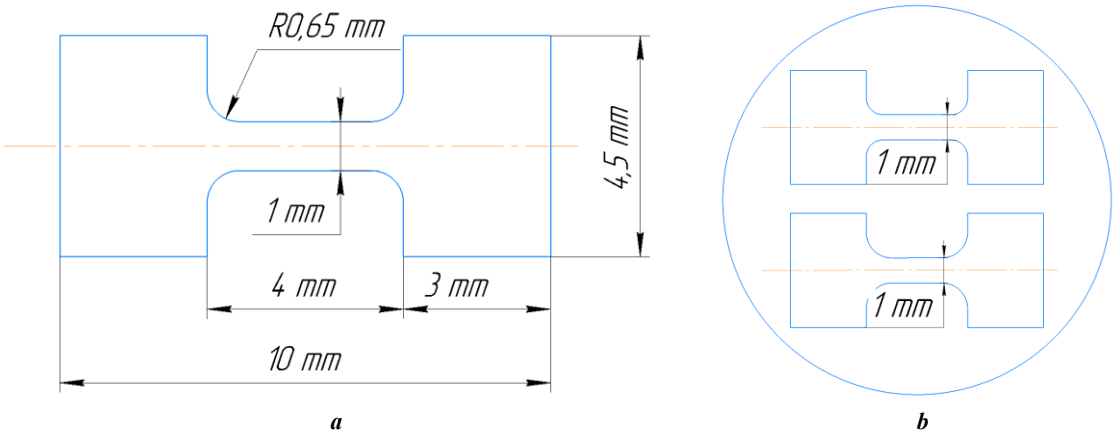

Fig. 1. *Shape of small samples for static tension tests:*
a *– drawing;* ***b*** *– layout of samples on the disk*
Рис. 1. *Форма малых образцов для испытаний на статическое растяжение:*
а *– чертеж;* ***b*** *– схема расположения образцов на диске*

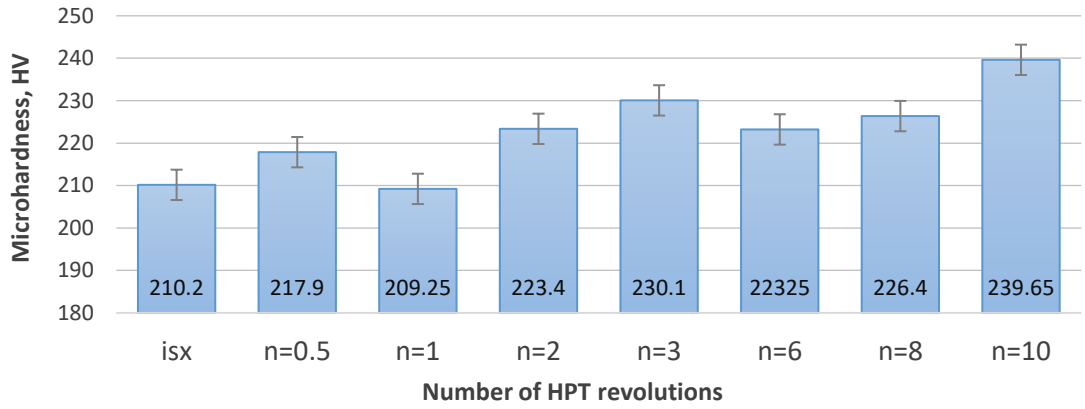

Fig. 2. *Microhardness of Zn–1%Fe–5%Mg samples after HPT with different number of revolutions*
Рис. 2. *Микротвердость образцов Zn–1%Fe–5%Mg после ИПДК с различным количеством оборотов*

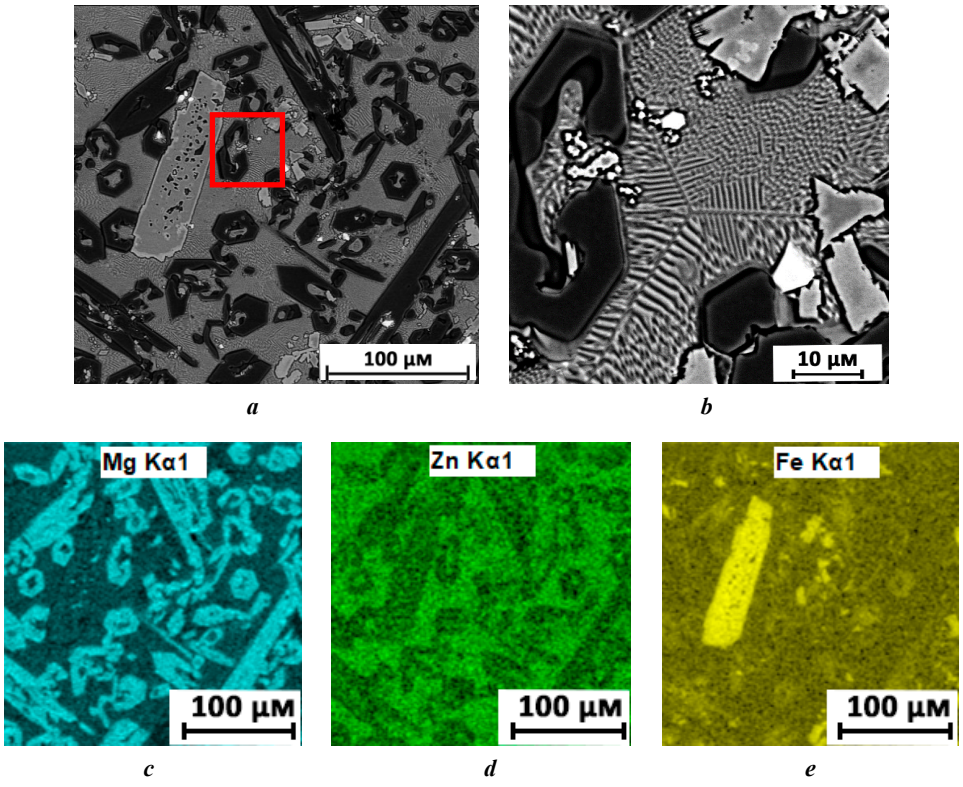

Fig. 3. *Structure of the Zn–1%Fe–5%Mg zinc alloy in the initial state (**a**, **b**) and EDS analysis of the Zn–1%Fe–5%Mg alloy (**c**–**e**)*
Рис. 3. *Структура цинкового сплава Zn–1%Fe–5%Mg в исходном состоянии (**a**, **b**) и EDS-анализ сплава Zn–1%Fe–5%Mg (**c**–**e**)*

$FeZn_{11}$ and $FeZn_{13}$ phases (light elements of irregular shape, hereinafter $FeZn_y$) and Fe and Mg content (dark elements of irregular shape), which is confirmed by EDS analysis (Fig. 3 c–e).

The structure after high-pressure torsion has undergone changes. The matrix is completely crushed; the fine-plate structure is transformed into ultra-fine-grained Mg_2Zn_{11}. The grain size is about 1 µm after 2 revolutions (Fig. 4 a). The solid phases Fe–Mg and $FeZn_y$ are crushed (Fig. 4 b). The results of EDS analysis (Fig. 4 c) showed that the dark-gray areas are the Fe–Mg phase, and the light-gray areas are pure zinc. After 8 revolutions, further refinement of the solid phases and their distribution throughout the entire sample volume are observed (Fig. 5). The volume fraction of the second phase did not change during deformation. Analysis of diffraction patterns showed (Fig. 6 a) that all X-ray spectra are characterized by the same set of intense peaks, and that the identified reflections belong to the Zn, $FeZn_{11}$ and $FeZn_{13}$, $MgZn_2$ and Mg_2Zn_{11} phases. There is a quantitative change in the ratio of peak intensities (Fig. 6 a), the profile shape, and the positions of the gravity centers of the X-ray peaks compared to the X-ray patterns of the corresponding initial state (Fig. 6 b). An increased integral

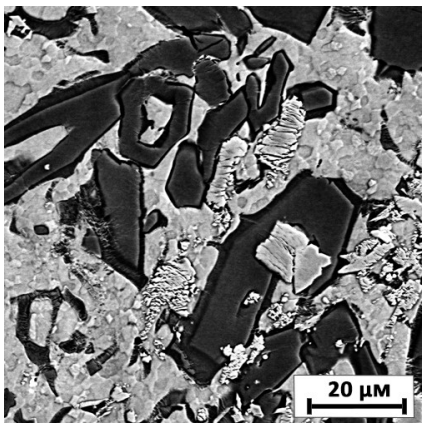

a

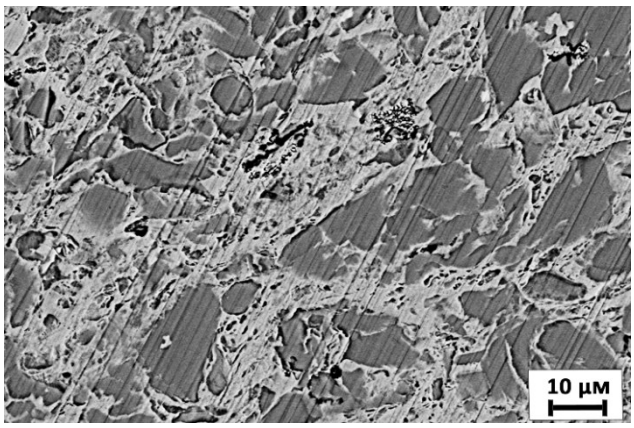

b

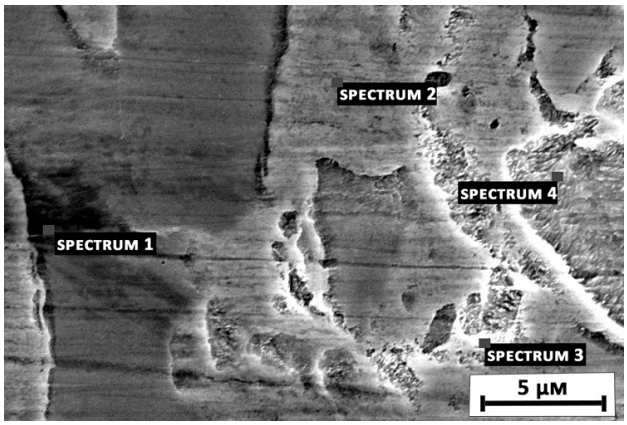

c

Spectrum	Mg	Fe	Zn	Total
Spectrum 1	15.19	0,47	84.33	100.00
Spectrum 2	0.00	0.00	100.00	100.00
Spectrum 3	1.06	0.00	98.94	100.00
Spectrum 4	13.92	0.42	85.67	100.00

Fig. 4. *Structure of the Zn–1%Fe–5%Mg zinc alloy after HPT for 2 revolutions:*
a *– SEM image at ×3000 magnification;* ***b*** *– SEM image at ×1000 magnification;* ***c*** *– EDS analysis of the Zn–1%Fe–5%Mg alloy*
Рис. 4. *Структура цинкового сплава Zn–1%Fe–5%Mg после ИПДК на 2 оборота:*
a *– РЭМ-изображение при увеличении ×3000;* ***b*** *– РЭМ-изображение при увеличении ×1000;* ***c*** *– EDS-анализ сплава Zn–1%Fe–5%Mg*

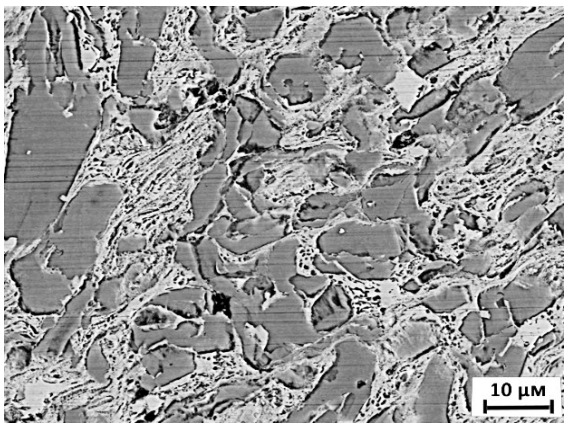

a

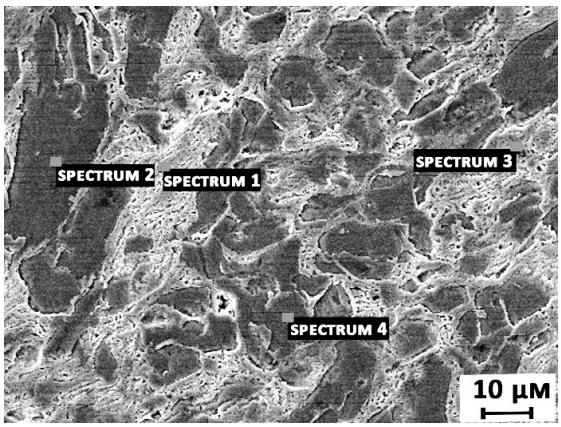

b

Spectrum	Mg	Fe	Zn	Total
Spectrum 1	1.51	0.89	97.60	100.00
Spectrum 2	15.09	2.41	82.50	100.00
Spectrum 3	0.00	0.00	100.00	100.00
Spectrum 4	13.54	2.04	84.42	100.00

Fig. 5. *Structure of the Zn–1%Fe–5%Mg zinc alloy after HPT for 8 revolutions:*
a *– SEM image;* ***b*** *– EDS analysis of the Zn–1%Fe–5%Mg alloy*
Рис. 5. *Структура цинкового сплава Zn–1%Fe–5%Mg после ИПДК на 8 оборотов:*
a *– РЭМ-изображение;* ***b*** *– EDS-анализ сплава Zn–1%Fe–5%Mg*

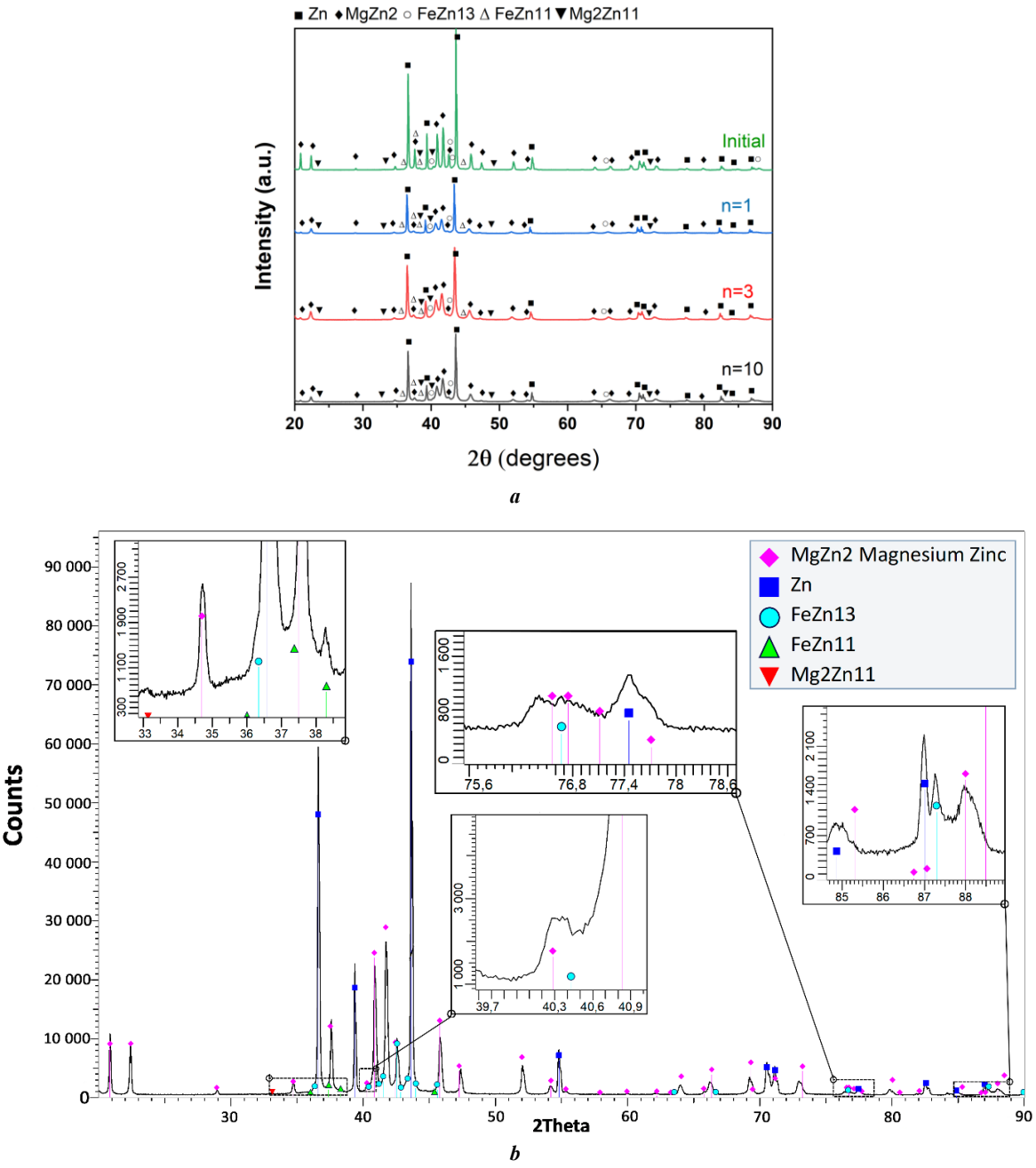

Fig. 6. *X-ray diffraction patterns of the Zn–1%Fe–5%Mg zinc alloy:* ***a*** *– before and after HPT;* ***b*** *– initial*
Рис. 6. *Рентгенограммы цинкового сплава Zn–1%Fe–5%Mg:* ***a*** *– до и после ИПДК;* ***b*** *– исходный*

intensity of the diffuse scattering background was detected (Fig. 6–8), which indicates changes in the identified phases and the occurrence of phase transitions in the alloy under study after high-pressure torsion treatment.

After 0.5 revolutions of high-pressure torsion, large particles with a size of approximately 40 μm are observed, most of them have an oblong shape and are elongated along one direction. After 3 revolutions, the structure begins to change significantly. The second phase particles are crushed and distributed throughout the entire volume. In the sample that underwent 8 revolutions of torsional deformation, the second phase particles were crushed to an average of 20 μm (Fig. 5 a), and after 10 revolutions – to 10 μm.

Corrosive characteristics

Corrosion destruction of a zinc alloy is determined by its heterogeneity in chemical and phase composition. Table 2 shows the influence of Ringer's solution during 60 days on the structure of the initial sample and the sample after high-pressure torsion for 10 revolutions. An increase in the corroded surface area is observed with increasing duration of the solution's influence on the samples, as well as a corrosion penetration deeper into the material, which correlates with the mass loss of the samples presented in Table 3. On the 10^{th} day, visible pores began to form in the original sample, which over time became larger. Fig. 9 presents photographs of the structure after 56 days of corrosion tests, where solid

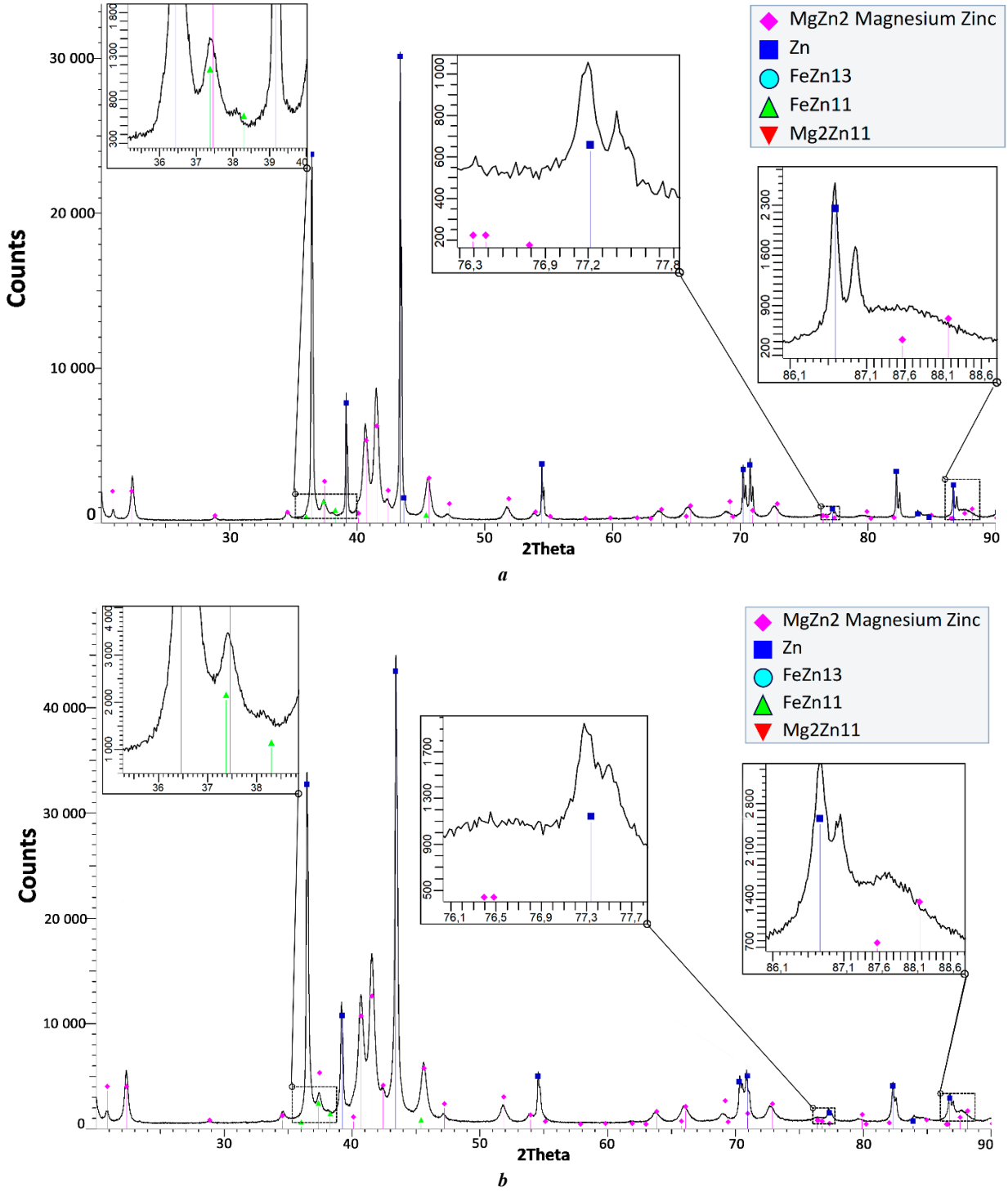

Fig. 7. *X-ray diffraction patterns of the Zn–1%Fe–5%Mg zinc alloy:* ***a*** *– after HPT for 1 revolution;* ***b*** *– after HPT for 3 revolutions*
Рис. 7. *Рентгенограммы цинкового сплава Zn–1%Fe–5%Mg:* ***а*** *– после ИПДК 1 на оборот;* ***b*** *– после ИПДК на 3 оборота*

particles in the initial state (Fig. 9 a) do not react with the solution; intercrystalline corrosion occurs when the active metal, in our case Mg, is a part of the matrix separating the metal crystalline grains. Corrosion in the original sample occurs in places where Mg is concentrated.

In a sample subjected to high-pressure torsion, similar cavities are observed after 28 days. In the deformed sample, corrosion proceeds visually more uniformly (Table 2 and Fig. 9 b), and mass loss occurs slightly faster than in the original (Table 3). Due to severe plastic deformation, the second phase containing Fe–Mg is refined and distributed throughout the entire volume of the sample. Refinement of structural elements using the method of severe plastic deformation promotes more uniform corrosion. The corrosion rate of the original sample on the 40th day of testing was 0.08 mm/year, on the 70th and 90th days – 0.13 mm/year. The corrosion rate of samples after HPT on the 40th day – 0.09 mm/year, on the 70th and 90th days – 0.15 mm/year.

On all HPT samples, pits are observed in the center that go deeper (Fig. 10 a), corrosion proceeds uniformly over

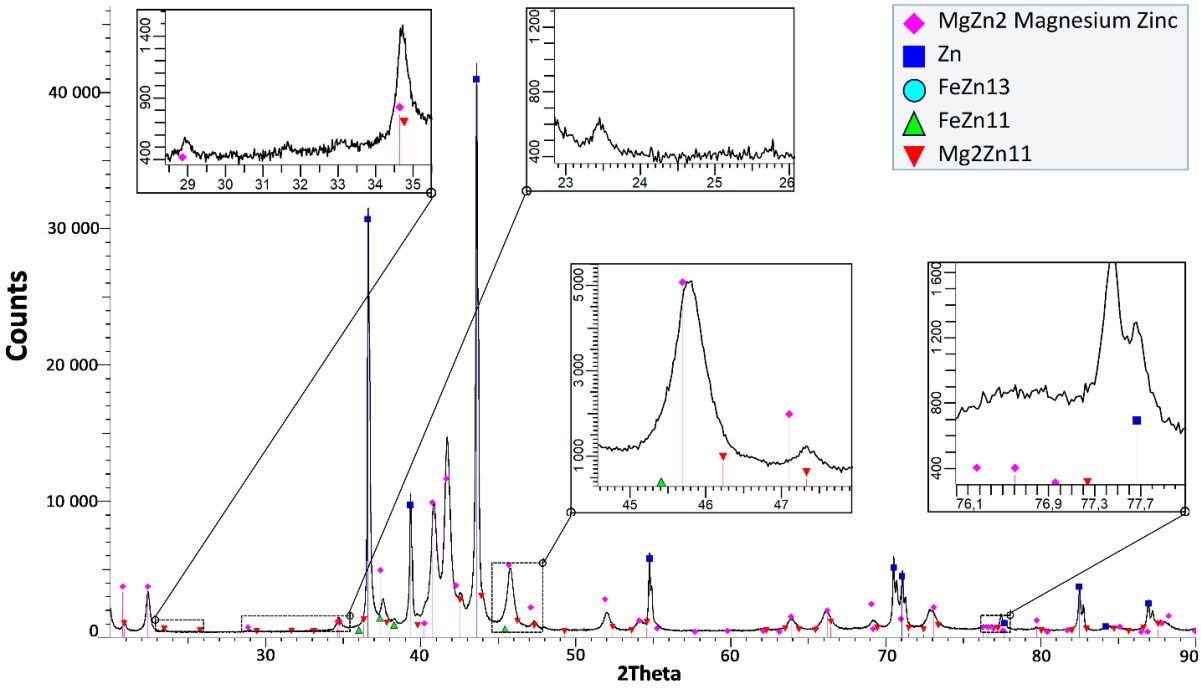

Fig. 8. *X-ray diffraction patterns of the Zn–1%Fe–5%Mg zinc alloy after HPT for 10 revolutions*
Рис. 8. *Рентгенограммы цинкового сплава Zn–1%Fe–5%Mg после ИПДК на 10 оборотов*

Table 2. *Photographs of the surface of samples after cleaning during corrosion tests*
Таблица 2. *Фотографии поверхности образцов после очистки в ходе коррозионных испытаний*

State	Test duration				
	2 days	10 days	25 days	40 days	60 days
Initial					
After HPT for 10 revolutions					

a larger area of the sample (Fig. 10 b). During HPT, a non-uniform structure is formed along the sample diameter. The grains take an elongated shape in the direction of torsion, since the angular rotation rate of the striker becomes greater with distance from the sample center, which affects the degree of material deformation, respectively, as well as the size of the structural elements and their orientations.

There were no gas emissions while the samples were in Ringer's solution.

Table 3. *Mass loss of samples during corrosion tests*
Таблица 3. *Потеря массы образцов во время коррозионных испытаний*

State	Test duration				
	1 day	10 days	25 days	40 days	60 days
Initial	0.55 %	1.55 %	2.21 %	2.88 %	4.31 %
After HPT for 10 revolutions	0.50 %	1.63 %	2.50 %	3.50 %	5.00 %

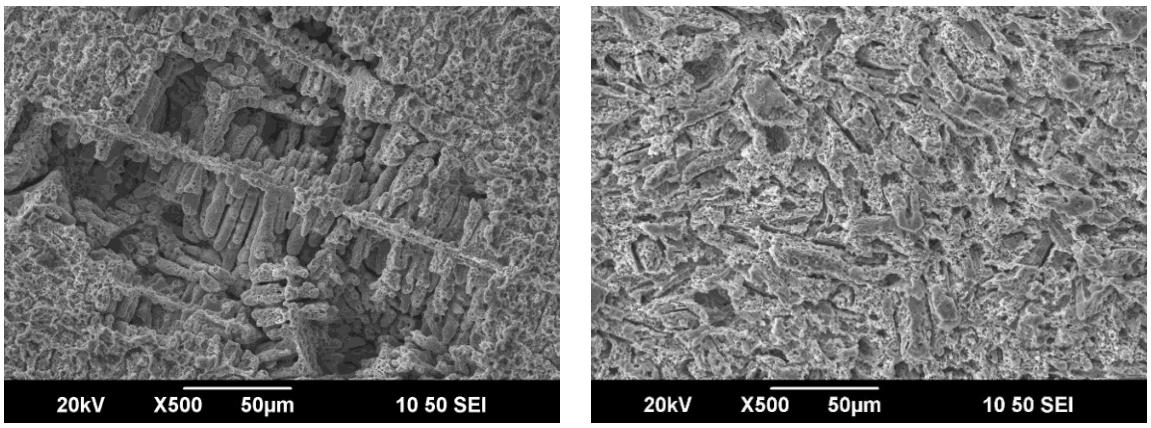

a ***b***

Fig. 9. *SEM images of the surface of samples of the Zn–1%Fe–5%Mg zinc alloy after 56 days of corrosion tests:* ***a*** *– initial;* ***b*** *– sample after 10 revolutions of HPT*
Рис. 9. *РЭМ-изображения поверхности образцов сплава Zn–1%Fe–5%Mg спустя 56 дней коррозионных испытаний:* ***a*** *– исходный;* ***b*** *– образец после 10 оборотов ИПДК*

DISCUSSION

In the initial state, the alloy consists of a eutectic matrix with a fine-plate α-Zn and Mg_2Zn_{11} structure (Fig. 3 b), which is also confirmed by X-ray diffraction analysis (Fig. 6 a). According to the Zn–Mg phase diagram [11], when Zn–Mg is cooled with a liquid containing 1 wt. % of Mg up to approximately 410 °C, the Zn phase first separates from the liquid. Next, at 364 °C the Mg_2Zn_{11} intermetallic compound appears. Thus, eutectics containing Zn and Mg_2Zn_{11} were formed along the boundaries of Zn grains. This is consistent with the results obtained in [12; 13]. Some small $MgZn_2$ peaks were detected (Fig. 6 b), which is likely related to the nonequilibrium solidification of Zn–Mg alloys during casting. Supercooling of the interdendritic liquid and deviation from the equilibrium diagram can lead to the $MgZn_2$ intermetallic compound precipitation in this alloy. A similar structure was observed in [14], where the Zn+Mg_2Zn_{11} eutectic, the needle $FeZn_{13}$ phase and the dendritic matrix Zn phase were present.

In the Zn–1%Fe–5%Mg alloy we studied, bright large $FeZn_{11}$ and $FeZn_{13}$ particles of irregular shape were also observed. X-ray spectral analysis detected two phases, but we could not separate them in the structure, so we left the designation $FeZn_y$. This elemental composition is also confirmed by EDS analysis. Except for this large phase, the structure contains dark-colored phases containing Fe and Mg (Fig. 3 c–e), but there are no cards with such content in the database of the program installed on the diffractometer.

In the Zn–Fe phase diagram, the temperature range of $FeZn_{13}$ formation by peritectic reaction is very wide and extends from 530 °C to room temperature, which may be the reason for the growth of $FeZn_{13}$ particles [14].

After severe plastic deformation, the solid Fe–Mg and $FeZn_y$ phases are crushed, and the matrix is completely refined. The fine-lamellar structure transforms into an ultrafine-grained structure with a grain size of about 1 μm after 2 revolutions (Fig. 4 a). A quantitative change in the ratio of the intensities of the Zn, $FeZn_{11}$ and $FeZn_{13}$, $MgZn_2$ and Mg_2Zn_{11} phase peaks (Fig. 6 a), the profile shape, the positions of the gravity centers of X-ray peaks, as well as the increased integral intensity of the diffuse scattering background (Fig. 7, 8) in comparison with radiographs of the corresponding initial state (Fig. 6 b) are observed. This indicates changes in the identified phases and the occurrence of phase transitions in the alloy under study as a result of high-pressure torsion.

There is no noticeable increase in microhardness after high-pressure torsion of a zinc alloy, but, unlike pure zinc [15] and other zinc alloys [16], the hardness of the considered Zn–1%Fe–5%Mg is the highest and reaches

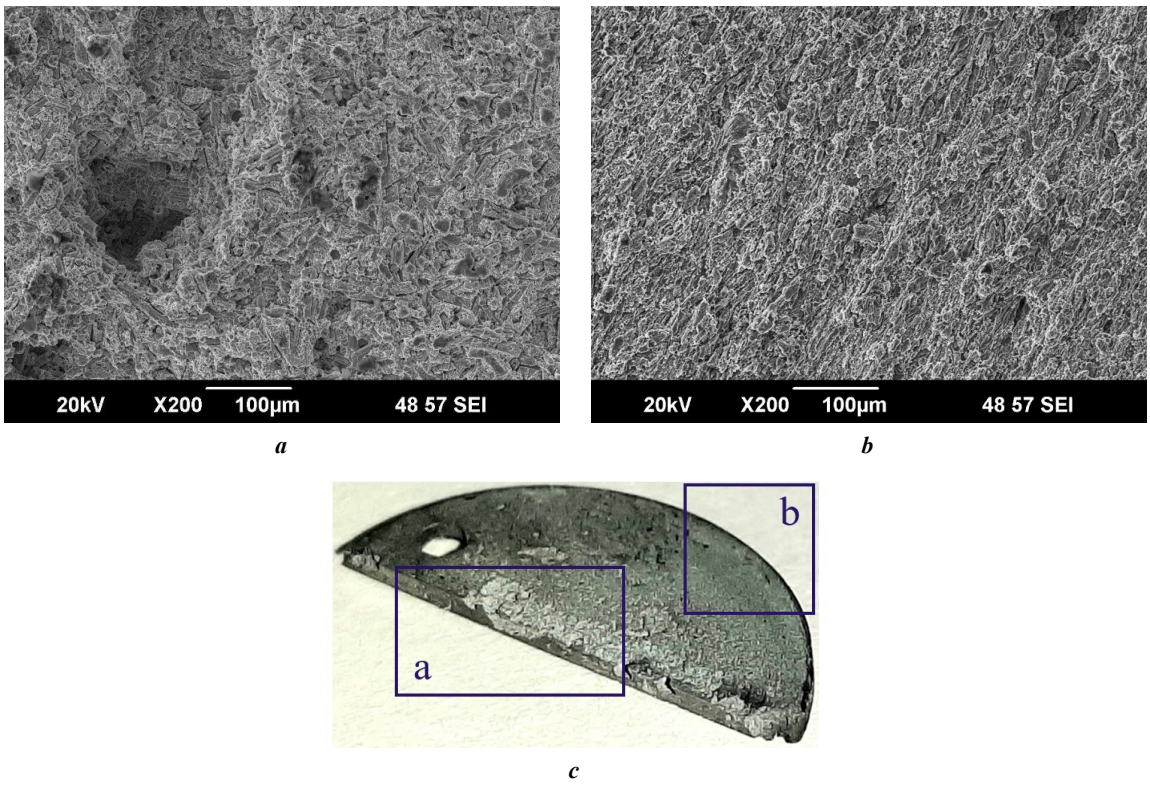

Fig. 10. *The structure of the sample subjected to 10 revolutions of HPT after 90 days of corrosion tests:* ***a*** *– central part of the sample;* ***b*** *– edge with changed texture;* ***c*** *– macroscopic image of the sample*
Рис. 10. *Структура образца, прошедшего 10 оборотов ИПДК, после 90 дней коррозионных испытаний:* ***a*** *– центральная часть образца;* ***b*** *– край с измененной текстурой;* ***c*** *– макроскопическое изображение образца*

210–240 HV due to alloying with Mg and Fe. The research in this work confirms that the Mg and Fe addition to a zinc alloy contributes to a significant increase in hardness values. In this case, the samples become very brittle.

The main deformation mechanism is glide of dislocations. In [14], measurements of the microhardness of the $FeZn_{13}$ and Mg_2Zn_{11} phases were made, which are 243±8 HV and 110±5 HV, respectively, with the Zn microhardness of 76.1 HV±2 HV, which leads to deformation incompatibility at the phase interface. Near the phase interface, a concentration of stresses and energy occurs, which causes dislocation glide and anomalous transformation determined by diffusion on moving defects (dislocations, grain boundaries) [17], and subsequently – dynamic Mg_2Zn_{11} phase recrystallization. Part of the stored energy was also released during $FeZn_{13}$ phase fragmentation.

The absence of gas emissions on the surface of the samples during corrosion tests is consistent with [14; 18]. When the samples were in the Ringer's solution, the pH of the corrosive environment gradually increased over time, which indicates the absorption of hydrogen ions in the solution, so the solution was often replenished during the experiment – every 48 h. A similar method of immersion test, where samples are cleaned every 24–48 h followed by repeated placement in a corrosive environment, was also used in works [19; 20]. This method allows estimating the rate of mass loss and corrosion rate for any time interval within 90 days. However, this method does not take into account the formation of a protective film and the change in corrosion rate due to passivation, so we plan to conduct continuous immersion tests.

The corrosion of zinc alloy is significantly higher than that of pure zinc, which is caused by the high potential difference between Mg_2Zn_{11} and $FeZn_{13}$. Corrosive destructions of a material depend on the metal activity; they easily react because they easily part with electrons at the external energy level. The degree of metal activity is characterized by the corresponding electrochemical series of metal stresses. Among the zinc alloy elements Zn (−0.76), Fe (−0.440), Mg (−2.363), Mg is the most active. Corrosion occurs in places where Mg is concentrated, since it has a more electronegative potential, therefore it acts as anodic centers and dissolves faster [21; 22]. $FeZn_{13}$ particles are cathodic and accelerate the dissolution of Zn and Mg-containing phases [23]. As in the study [24], an acceleration of corrosion processes in samples after high-pressure torsion is observed. The formation of a heterogeneous structure in the sample is consistent with [25]. The formation of visible corrosion pits in the center of HPT samples is determined by different crystallographic grain orientations in the HCP-lattice metal. A similar dependence was also reported in [26; 27].

The study of the mechanical properties and microstructure of the zinc alloy allows evaluating the prospects for its further research in vitro and in vivo for application as a material for the production of medical implants.

CONCLUSIONS

As a result of processing the Zn–1%Fe–5%Mg alloy by high-pressure torsion, samples with high hardness values (up to 239 MPa), but very brittle, were obtained.

The structure of the zinc alloy is multiphase; it contains $FeZn_{11}$, $FeZn_{13}$ and Mg–Fe solid particles, which are destroyed and partially dissolved during high-pressure torsion. The solid phases are located in a matrix of Zn and Mg_2Zn_{11}, which is transformed during the high-pressure torsion process into equiaxial grains of 1 μm in size.

The use of high-pressure torsion does not lead to significant changes in the corrosion rate, but leads to more uniform corrosion throughout the volume of the sample. The exception is the center with a less developed structure, where an intense penetration is observed.

REFERENCES

1. Kogan S., Sood A., Granick M.S. Zinc and Wound Healing: A Review of Zinc Physiology and Clinical Applications. *Wounds*, 2017, vol. 29, no. 4, pp. 102–106.
2. Lin Mao, Li Shen, Jiahui Chen et al. A promising biodegradable magnesium alloy suitable for clinical vascular stent application. *Scientific Reports*, 2017, vol. 7, article number 46343. DOI: 10.1038/srep46343.
3. Yang Hongtao, Jia Bo, Zhang Zechuan, Qu Xinhua, Li Guannan, Lin Wenjiao, Zhu Donghui, Dai Kerong, Zheng Yufeng. Alloying design of biodegradable zinc as promising bone implants for load-bearing applications. *Nature Communications*, 2020, vol. 11, article number 401. DOI: 10.1038/s41467-019-14153-7.
4. Shi Zhangzhi, Li Changheng, Li Meng, Li Xiangmin, Wang Luning. Second phase refining induced optimization of Fe alloying in Zn: Significantly enhanced strengthening effect and corrosion uniformity. *International Journal Minerals, Metallurgy and Materials*, 2022, vol. 29, pp. 796–806. DOI: 10.1007/s12613-022-2468-6.
5. Mita K., Ikeda T., Maeda M. Phase diagram study of Fe–Zn intermetallics. *Journal of Phase Equilibria*, 2001, vol. 22, pp. 122–125. DOI: 10.1361/105497101770338978.
6. Su Yingchao, Fu Jiayin, Lee Wonsae, Du Shaokang, Qin Yi-Xian, Zheng Yufeng, Wang Yadong, Zhu Donghui. Improved mechanical, degradation, and biological perfomaces of Zn–Fe alloys as bioresorbable implants. *Bioactive Materials*, 2022, vol. 17, pp. 334–343. DOI: 10.1016/j.bioactmat.2021.12.030.
7. Shao Xiaoxi, Wang Xiang, Xu Fangfang et al. In vivo biocompatibility and degradability of a Zn–Mg–Fe alloy osteosynthesis system // Bioactive Materials. 2022. Vol. 7. P. 154–166. DOI: 10.1016/j.bioactmat.2021.05.012.
8. Mostaed E., Sikora-Jasinska M., Mostaed A., Loffredo S., Demir A.G., Previtali B., Mantovani D., Beanland R., Vedani M. Novel Zn-based alloys for biodegradable stent applications: Design, development and in vitro degradation // Journal of the Mechanical Behavior of Biomedical Materials. 2016. Vol. 60. P. 581–602. DOI: 10.1016/j.jmbbm.2016.03.018.
9. Vojtěch D., Kubásek J., Šerák J., Novák P. Mechanical and corrosion properties of newly developed biodegradable Zn-based alloys for bone fixation. *Acta Biomaterialia*, 2011, vol. 7, no. 9, pp. 3515–3522. DOI: 10.1016/j.actbio.2011.05.008.
10. Valiev R.Z., Islamgaliev R.K., Alexandrov I.V. Bulk nanostructured materials from severe plastic deformation. *Progress in Materials Science*, 2000, vol. 45, no. 2, pp. 103–189. DOI: 10.1016/S0079-6425(99)00007-9.
11. Li Baoping, Dong Anping, Zhu Guoliang, Chu Shuangjie, Qian Hongwei, Hu Chengjie, Sun Baode, Wang Jun. Investigation of the corrosion behaviors of continuously hot-dip galvanizing Zn–Mg coating. *Surface and Coatings Technology*, 2012, vol. 206, no. 19-20, pp. 3989–3999. DOI: 10.1016/j.surfcoat.2012.03.079.
12. Prosek T., Nazarov A., Bexell U., Thierry D., Serak J. Corrosion mechanism of model zinc–magnesium alloys in atmospheric conditions. *Corrosion Science*, 2008, vol. 50, no. 8, pp. 2216–2231. DOI: 10.1016/j.corsci.2008.06.008.
13. Xue Penghao, Ma Minglong, Li Yongjun, Li Xinggang, Yuan Jiawei, Shi Guoliang, Wang Kaikun, Zhang Kui. Microstructure, Hot Deformation Behavior, and Recrystallization Behavior of Zn–1Fe–1Mg Alloy under Isothermal Compression. *Materials*, 2021, vol. 14, no. 7, article number 1735. DOI: 10.3390/ma14071735.
14. Xue Penghao, Ma Minglong, Li Yongjun, Li Xinggang, Yuan Jiawei, Shi Guoliang, Wang Kaikun, Zhang Kui. Microstructure, Mechanical Properties, and In Vitro Corrosion Behavior of Biodegradable Zn–1Fe–xMg Alloy. *Materials*, 2020, vol. 13, no. 21, article number 4835. DOI: 10.3390/ma13214835.
15. Polenok M.V., Khafizova E.D., Islamgaliev R.K. The influence of severe plastic deformation on mechanical properties of pure zinc. *Frontier Materials & Technologies*, 2022, no. 3-2, pp. 25–31. DOI: 10.18323/2782-4039-2022-3-2-25-31.
16. Mostaed E., Sikora-Jasinska M., Drelich J.W., Vedani M. Zinc-based alloys for degradable vascular stent application. *Acta Biomaterialia*, 2018, vol. 71, pp. 1–23. DOI: 10.1016/j.actbio.2018.03.005.
17. Razumov I.K., Ermakov A.Y., Gornostyrev Yu.N., Straumal B.B. Nonequilibrium phase transformations in alloys under severe plastic deformation. *Physics-Uspekhi*, 2020, vol. 63, no. 8, pp. 733–757. DOI: DOI: 10.3367/UFNe.2019.10.038671.
18. Zhang Xiaoge Gregory. Corrosion potential and corrosion current. *Corrosion and Electrochemistry of Zinc*. Boston, Springer Publ., 1996, pp. 125–156. DOI: 10.1007/978-1-4757-9877-7_5.
19. Khudododova G.D., Kulyasova O.B., Islamgaliev R.K. Strength and corrosion resistance of the UFG Mg-Zn-Ca alloy. *Nanoindustriya*, 2022, vol. 15, no. 7-8, pp. 426–433. DOI: 10.22184/1993-8578.2022.15.7-8.426.433.
20. Byun Jong Min, Yu Jin Min, Kim Dae Kyung, Kim Tae Yeob, Jun Woo Sung, Kim Young Do. Corrosion Behavior of Mg_2Zn_{11} and $MgZn_2$ Single Phases. *Korean Journal of Metals and Materials*, 2013, vol. 51, no. 6, pp. 413–419. DOI: 10.3365/KJMM.2013.51.6.413.
21. Wątroba M., Mech K., Bednarczyk W., Kawałko J., Marciszko-Wiąckowska M., Marzec M., Shepherd D.E.T., Bała P. Long-term in vitro corrosion behavior of Zn–3Ag and Zn–3Ag–0.5Mg alloys considered for biodegradable implant applications. *Materials & Design*, 2022, vol. 213, article number 110289. DOI: 10.1016/j.matdes.2021.110289.

22. Bowen P.K., Shearier E.R., Shan Zhao, Guillory R.J., Feng Zhao, Goldman J., Drelich J.W. Biodegradable Metals for Cardiovascular Stents: from Clinical Concerns to Recent Zn-Alloys. *Advanced Healthcare Materials*, 2016, vol. 5, no. 10, pp. 1121–1140. DOI: 10.1002/adhm.201501019.
23. Shi Zhang-Zhi, Gao Xi-Xian, Chen Hong-Ting, Liu Xue-Feng, Li Ang, Zhang Hai-Jun, Wang Lu-Ning. Enhancement in mechanical and corrosion resistance properties of a biodegradable Zn–Fe alloy through second phase refinement. *Materials Science and Engineering: C*, 2020, vol. 116, article number 111197. DOI: 10.1016/j.msec.2020.111197.
24. Yan Zhaoming, Zhu Jiaxuan, Zhang Zhimin, Wang Qiang, Xue Yong. The microstructural, textural, and mechanical effects of high-pressure torsion processing on Mg alloys: A review. *Frontiers in Materials*, 2022, vol. 9, article number 964992. DOI: 10.3389/fmats.2022.964992.
25. Myagkikh P.N., Merson E.D., Poluyanov V.A., Merson D.L. The dependence of the biodegradable ZX10 alloy corrosion process on the structural factors and local pH level. *Frontier Materials & Technologies*, 2023, no. 2, pp. 59–76. DOI: 10.18323/2782-4039-2023-2-64-3.
26. Vinogradov A., Merson E., Myagkikh P., Linderov M., Brilevsky A., Merson D. Attaining High Functional Performance in Biodegradable Mg-Alloys: An Overview of Challenges and Prospects for the Mg–Zn–Ca System. *Materials*, 2023, vol. 16, no. 3, article number 1324. DOI: 10.3390/ma16031324.
27. Yao Caizhen, Wang Zichao, Tay See Leng, Zhu Tianping, Gao Wei. Effects of Mg on microstructure and corrosion properties of Zn–Mg alloy. *Journal of Alloys and Compounds*, 2014, vol. 602, pp. 101–107. DOI: 10.1016/j.jallcom.2014.03.025.

СПИСОК ЛИТЕРАТУРЫ

1. Kogan S., Sood A., Granick M.S. Zinc and Wound Healing: A Review of Zinc Physiology and Clinical Applications // Wounds. 2017. Vol. 29. № 4. P. 102–106.
2. Lin Mao, Li Shen, Jiahui Chen et al. A promising biodegradable magnesium alloy suitable for clinical vascular stent application // Scientific Reports. 2017. Vol. 7. Article number 46343. DOI: 10.1038/srep46343.
3. Yang Hongtao, Jia Bo, Zhang Zechuan, Qu Xinhua, Li Guannan, Lin Wenjiao, Zhu Donghui, Dai Kerong, Zheng Yufeng. Alloying design of biodegradable zinc as promising bone implants for load-bearing applications // Nature Communications. 2020. Vol. 11. Article number 401. DOI: 10.1038/s41467-019-14153-7.
4. Shi Zhangzhi, Li Changheng, Li Meng, Li Xiangmin, Wang Luning. Second phase refining induced optimization of Fe alloying in Zn: Significantly enhanced strengthening effect and corrosion uniformity // International Journal Minerals, Metallurgy and Materials. 2022. Vol. 29. P. 796–806. DOI: 10.1007/s12613-022-2468-6.
5. Mita K., Ikeda T., Maeda M. Phase diagram study of Fe–Zn intermetallics // Journal of Phase Equilibria. 2001. Vol. 22. P. 122–125. DOI: 10.1361/105497101770338978.
6. Su Yingchao, Fu Jiayin, Lee Wonsae, Du Shaokang, Qin Yi-Xian, Zheng Yufeng, Wang Yadong, Zhu Donghui. Improved mechanical, degradation, and biological perfomaces of Zn–Fe alloys as bioresorbable implants // Bioactive Materials. 2022. Vol. 17. P. 334–343. DOI: 10.1016/j.bioactmat.2021.12.030.
7. Shao Xiaoxi, Wang Xiang, Xu Fangfang et al. In vivo biocompatibility and degradability of a Zn–Mg–Fe alloy osteosynthesis system // Bioactive Materials. 2022. Vol. 7. P. 154–166. DOI: 10.1016/j.bioactmat.2021.05.012.
8. Mostaed E., Sikora-Jasinska M., Mostaed A., Loffredo S., Demir A.G., Previtali B., Mantovani D., Beanland R., Vedani M. Novel Zn-based alloys for biodegradable stent applications: Design, development and in vitro degradation // Journal of the Mechanical Behavior of Biomedical Materials. 2016. Vol. 60. P. 581–602. DOI: 10.1016/j.jmbbm.2016.03.018.
9. Vojtěch D., Kubásek J., Šerák J., Novák P. Mechanical and corrosion properties of newly developed biodegradable Zn-based alloys for bone fixation // Acta Biomaterialia. 2011. Vol. 7. № 9. P. 3515–3522. DOI: 10.1016/j.actbio.2011.05.008.
10. Valiev R.Z., Islamgaliev R.K., Alexandrov I.V. Bulk nanostructured materials from severe plastic deformation // Progress in Materials Science. 2000. Vol. 45. № 2. P. 103–189. DOI: 10.1016/S0079-6425(99)00007-9.
11. Li Baoping, Dong Anping, Zhu Guoliang, Chu Shuangjie, Qian Hongwei, Hu Chengjie, Sun Baode, Wang Jun. Investigation of the corrosion behaviors of continuously hot-dip galvanizing Zn–Mg coating // Surface and Coatings Technology. 2012. Vol. 206. № 19-20. P. 3989–3999. DOI: 10.1016/j.surfcoat.2012.03.079.
12. Prosek T., Nazarov A., Bexell U., Thierry D., Serak J. Corrosion mechanism of model zinc–magnesium alloys in atmospheric conditions // Corrosion Science. 2008. Vol. 50. № 8. P. 2216–2231. DOI: 10.1016/j.corsci.2008.06.008.
13. Xue Penghao, Ma Minglong, Li Yongjun, Li Xinggang, Yuan Jiawei, Shi Guoliang, Wang Kaikun, Zhang Kui. Microstructure, Hot Deformation Behavior, and Recrystallization Behavior of Zn–1Fe–1Mg Alloy under Isothermal Compression // Materials. 2021. Vol. 14. № 7. Article number 1735. DOI: 10.3390/ma14071735.
14. Xue Penghao, Ma Minglong, Li Yongjun, Li Xinggang, Yuan Jiawei, Shi Guoliang, Wang Kaikun, Zhang Kui. Microstructure, Mechanical Properties, and In Vitro Corrosion Behavior of Biodegradable Zn–1Fe–xMg Alloy // Materials. 2020. Vol. 13. № 21. Article number 4835. DOI: 10.3390/ma13214835.
15. Поленок М.В., Хафизова Э.Д., Исламгалиев Р.К. Влияние интенсивной пластической деформации на механические свойства чистого цинка // Frontier Materials & Technologies. 2022. № 3-2. С. 25–31. DOI: 10.18323/2782-4039-2022-3-2-25-31.
16. Mostaed E., Sikora-Jasinska M., Drelich J.W., Vedani M. Zinc-based alloys for degradable vascular stent application // Acta Biomaterialia. 2018. Vol. 71. P. 1–23. DOI: 10.1016/j.actbio.2018.03.005.
17. Разумов И.К., Ермаков А.Е., Горностырев Ю.Н., Страумал Б.Б. Неравновесные фазовые превращения в сплавах // Успехи физических наук. 2019. Т. 190. № 8. С. 785–810. DOI: 10.3367/UFNr.2019.10.038671.
18. Zhang Xiaoge Gregory. Corrosion potential and corrosion current // Corrosion and Electrochemistry of Zinc. Boston: Springer, 1996. P. 125–156. DOI: 10.1007/978-1-4757-9877-7_5.

19. Худододова Г.Д., Кулясова О.Б., Исламгалиев Р.К. Прочностные и коррозионные свойства УМЗ-сплава Mg–Zn–Ca // Наноиндустрия. 2022. Т. 15. № 7-8. С. 426–433. DOI: 10.22184/1993-8578.2022.15.7-8.426.433.
20. Byun Jong Min, Yu Jin Min, Kim Dae Kyung, Kim Tae Yeob, Jun Woo Sung, Kim Young Do. Corrosion Behavior of Mg_2Zn_{11} and $MgZn_2$ Single Phases // Korean Journal of Metals and Materials. 2013. Vol. 51. № 6. P. 413–419. DOI: 10.3365/KJMM.2013.51.6.413.
21. Wątroba M., Mech K., Bednarczyk W., Kawałko J., Marciszko-Wiąckowska M., Marzec M., Shepherd D.E.T., Bała P. Long-term in vitro corrosion behavior of Zn–3Ag and Zn–3Ag–0.5Mg alloys considered for biodegradable implant applications // Materials & Design. 2022. Vol. 213. Article number 110289. DOI: 10.1016/j.matdes.2021.110289.
22. Bowen P.K., Shearier E.R., Shan Zhao, Guillory R.J., Feng Zhao, Goldman J., Drelich J.W. Biodegradable Metals for Cardiovascular Stents: from Clinical Concerns to Recent Zn-Alloys // Advanced Healthcare Materials. 2016. Vol. 5. № 10. P. 1121–1140. DOI: 10.1002/adhm.201501019.
23. Shi Zhang-Zhi, Gao Xi-Xian, Chen Hong-Ting, Liu Xue-Feng, Li Ang, Zhang Hai-Jun, Wang Lu-Ning. Enhancement in mechanical and corrosion resistance properties of a biodegradable Zn–Fe alloy through second phase refinement // Materials Science and Engineering: C. 2020. Vol. 116. Article number 111197. DOI: 10.1016/j.msec.2020.111197.
24. Yan Zhaoming, Zhu Jiaxuan, Zhang Zhimin, Wang Qiang, Xue Yong. The microstructural, textural, and mechanical effects of high-pressure torsion processing on Mg alloys: A review // Frontiers in Materials. 2022. Vol. 9. Article number 964992. DOI: 10.3389/fmats.2022.964992.
25. Мягких П.Н., Мерсон Е.Д., Полуянов В.А., Мерсон Д.Л. Зависимость процесса коррозии биорезорбируемого сплава ZX10 от структурных факторов и локального уровня pH // Frontier Materials & Technologies. 2023. № 2. С. 59–76. DOI: 10.18323/2782-4039-2023-2-64-3.
26. Vinogradov A., Merson E., Myagkikh P., Linderov M., Brilevsky A., Merson D. Attaining High Functional Performance in Biodegradable Mg-Alloys: An Overview of Challenges and Prospects for the Mg–Zn–Ca System // Materials. 2023. Vol. 16. № 3. Article number 1324. DOI: 10.3390/ma16031324.
27. Yao Caizhen, Wang Zichao, Tay See Leng, Zhu Tianping, Gao Wei. Effects of Mg on microstructure and corrosion properties of Zn–Mg alloy // Journal of Alloys and Compounds. 2014. Vol. 602. P. 101–107. DOI: 10.1016/j.jallcom.2014.03.025.

Влияние интенсивной пластической деформации кручением на структуру и механические свойства цинкового сплава Zn–1%Fe–5%Mg

Абдрахманова Эльмира Дамировна[1], студент
Хафизова Эльвира Динифовна*[2], кандидат технических наук,
доцент кафедры материаловедения и физики металлов, старший научный сотрудник
научно-исследовательской лаборатории «Металлы и сплавы при экстремальных воздействиях»
Поленок Милена Владиславовна[3], студент
Нафиков Руслан Камилович[4], младший научный сотрудник
научно-исследовательской лаборатории «Металлы и сплавы при экстремальных воздействиях»
Корзникова Елена Александровна[5], доктор физико-математических наук, профессор,
профессор кафедры материаловедения и физики металлов,
заведующий научно-исследовательской лабораторией «Металлы и сплавы при экстремальных воздействиях»
Уфимский университет науки и технологий, Уфа (Россия)

***E-mail:** KhafizovaED@uust.ru,
ela.90@mail.ru

[1]ORCID: https://orcid.org/0009-0009-2775-7488
[2]ORCID: https://orcid.org/0000-0002-4618-412X
[3]ORCID: https://orcid.org/0000-0001-9774-1689
[4]ORCID: https://orcid.org/0000-0003-1280-6258
[5]ORCID: https://orcid.org/0000-0002-5975-4849

Поступила в редакцию 27.06.2023 *Принята к публикации 06.03.2024*

Аннотация: В настоящее время ведутся поиски новых материалов для временных имплантатов, способных растворяться в организме, что приводит к исчезновению потребности в повторной операции. В последнее десятилетие интерес ученых был сосредоточен на материалах на основе цинка, так как он, в отличие от других металлов, имеет подходящую скорость коррозии и хорошую биосовместимость. В работе описан эксперимент по изучению влияния деформации на микроструктуру, прочностные и коррозионные свойства сплава системы Zn–Fe–Mg. Проведен энергодисперсионный анализ и расчет объемной доли второй фазы цинкового сплава Zn–Fe–Mg. Гравиметрическим методом исследованы коррозионные свойства цинкового сплава Zn–Fe–Mg с разной микроструктурой (до и после интенсивной пластической деформации кручением) в условиях, имитирующих условия внутри живого организма (температура, состав коррозионной среды). В ходе испытаний определен механизм протекания коррозии, рассчитаны ее скорость и потеря массы образцов. Проведены исследования рельефа коррозионной поверхности методом растровой электронной микроскопии. Установлено, что разрушение материала в коррозионной среде происходит по матрице, содержащей активный металл Mg. Результаты расчетов скорости коррозии у исходного

и ИПДК-образцов отличались из-за более равномерного распределения частиц второй фазы во время интенсивной пластической деформации. В данной работе методом легирования цинка железом и магнием, а также применением интенсивной пластической деформации кручением получилось повысить микротвердость образцов до 239,6±8 HV, что является высоким показателем для цинковых сплавов.

Ключевые слова: цинковые сплавы; Zn–Fe–Mg; биодеградируемые имплантаты; интенсивная пластическая деформация кручением; биосовместимые материалы.

Благодарности: Исследования выполнены за счет средств гранта в области науки из бюджета Республики Башкортостан для государственной поддержки молодых ученых (НОЦ-ГМУ-2022, Соглашение № 1 от 13.12.2022).

Работа Корзниковой Е.А., Нафикова Р.К. выполнена при финансовой поддержке Министерства науки и высшего образования РФ в рамках государственного задания на оказание государственных услуг ФГБОУ ВО УУНиТ (соглашение № 075-03-2024-123/1) «Молодежная научно-исследовательская лаборатория НОЦ "Металлы и сплавы при экстремальных воздействиях"».

Исследовательская часть работы выполнена с использованием оборудования ЦКП «Нанотех» ФГБОУ ВО УУНиТ.

Статья подготовлена по материалам докладов участников XI Международной школы «Физическое материаловедение» (ШФМ-2023), Тольятти, 11–15 сентября 2023 года.

Для цитирования: Абдрахманова Э.Д., Хафизова Э.Д., Поленок М.В., Нафиков Р.К., Корзникова Е.А. Влияние интенсивной пластической деформации кручением на структуру и механические свойства цинкового сплава Zn–1%Fe–5%Mg // Frontier Materials & Technologies. 2024. № 2. С. 9–22. DOI: 10.18323/2782-4039-2024-2-68-1.